Modulating Emission Properties in a Host–Guest Colloidal Quantum Well Superlattice

Junhong Yu, Manoj Sharma, Yimeng Wang, Savas Delikanli, Hamed Dehghanpour Baruj, Ashma Sharma, Hilmi Volkan Demir,* and Cuong Dang*

Self-assembly of colloidal nanocrystals into ordered superlattices is a powerful approach to enable novel collective properties which are not available in individual colloids. However, to date, it remains a major challenge to develop a practical route to modulate such collective properties for potential photonic applications. Herein, it is shown that the collective emission properties in colloidal quantum well (CQW) superlattices, including emission color and anisotropy, can be effectively modulated in a binary host–guest architecture. The experimental and theoretical results reveal that excitons of the host (i.e., the undoped CQWs) generated by photoexcitation can be controllably harvested by the guest (i.e., the Cu-doped CQWs) for light emission, owing to an exciton hopping assisted exciton trapping process. Such a nano-building block with tunable collective optical properties may enlighten novel colloidal material-based photonic applications, including optical anti-counterfeiting, next-generation liquid crystal displays, and multifunctional biological markers.

J. Yu, M. Sharma, Y. Wang, S. Delikanli, A. Sharma, H. V. Demir, C. Dang
LUMINOUS! Centre of Excellence for Semiconductor Lighting and
Displays
School of Electrical and Electronic Engineering
The Photonics Institute (TPI)
Nanyang Technological University
50 Nanyang Avenue, Singapore 639798, Singapore
E-mail: volkan@stanfordalumni.org; hcdang@ntu.edu.sg

M. Sharma, S. Delikanli, H. D. Baruj, H. V. Demir
Department of Electrical and Electronics Engineering and Department
of Physics
UNAM Institute of Materials Science and Nanotechnology
Bilkent University
Bilkent, Ankara 06800, Turkey

M. Sharma
ARC Centre of Excellence in Exciton Science
Department of Materials Science and Engineering
Monash University
Clayton Campus, Melbourne, Victoria 3800, Australia

H. V. Demir
School of Physical and Mathematical Sciences
Division of Physics and Applied Physics
Nanyang Technological University
Singapore 639798, Singapore

C. Dang
CINTRA UMI CNRS/NTU/THALES 3288
Research Techno Plaza
50 Nanyang Drive, Border X Block, Level 6, Singapore 637553, Singapore

The ORCID identification number(s) for the author(s) of this article
can be found under https://doi.org/10.1002/adom.202101756.

1. Introduction

Superlattices constructed by colloidal nanocrystals, which mimic the organization of atoms into a crystal and exhibit unique ensemble properties, have attracted tremendous research interests for the design of novel functional materials.[1–4] Besides the common advantages of the colloidal nanocrystal family to be ingredients to construct superlattices,[5,6] such as wide tunability in geometry/ physical properties and easy-to-handle colloidal states, colloidal quantum wells (CQW) have demonstrated exceptional photophysical properties benefitting from the atomically flat nanostructure and its magic-sized vertical thickness.[7–14] These characteristics, including spectrally pure light emission,[7,8] preferential interactions between the platelet planes,[9–11] and a highly anisotropic electronic structure,[12–14] have highlighted CQWs as a promising type of building blocks to generate superlattices targeting for photonic applications.

So far, considerable progress in the investigations of CQW superlattices has been made by different groups.[9,10,15–20] Long anisotropic CQW superlattices beyond 10 μm have been observed, and the collective properties of the ordered superlattices have been characterized. For example, Murray et al. demonstrated that the self-assembly of CQWs can be directed into ordered superlattices at the liquid–air interface.[15,16] Tisdale et al.[13] and Riedinger et al.[18] revealed that the orientation of CQWs in the superlattice can be controlled by engineering the solvent. Dubertret et al. showed that the self-assembly of CQWs into stacked columnar structures displays polarized emission[9] and a phonon-replica line at low temperature.[10] However, the majority of these efforts on CQW superlattices have focused on structure constructions and understandings of emerging properties. To functionalize the CQW superlattices for photonic applications, it is often desirable to self-assemble the CQWs into a superlattice with programmable collective properties.[21] Unfortunately, this controllability has remained elusive and a daunting challenge to date.

In this work, we propose a binary host–guest superlattice constructed by four monolayers (MLs) CdSe undoped (the host) and Cu-doped CQWs (the guest) to demonstrate the modulation of collective emission properties. Experimental results reveal that the presence of even a few guest ingredients can strongly

modify the preference of exciton recombination channel via band-edge emission (BE) or copper emission (CE) due to an ultralong exciton hopping range (>100 nm)[17,20] and an ultrafast exciton hopping rate (≈4 ps).[11,17,22] By enlarging the vertical dimension of the binary superlattice, more photoexcited excitons are harvested by Cu dopants and as a result, the greenish and anisotropy photoluminescence (the intrinsic emission properties of BE)[12,13] is gradually changed into the reddish and isotropy photoluminescence (the intrinsic emission properties of CE).[22,23] In addition, we have modeled the excitonic dynamics (including exciton transfer, exciton trapping, and exciton recombination) in the binary superlattice, which can well-reproduce the controllability observed in the experiments. This work, which expands the current understanding of manipulating collective properties in colloidal superlattices, could lead to novel photonic applications such as multimode optical anticounterfeiting, next-generation liquid crystal displays, and multifunctional biological markers.

2. Results and Discussion

Undoped CdSe CQWs with a vertical thickness of 1.2 nm corresponding to four MLs of lattice unit are synthesized according to previously reported procedures.[7,24] After thorough purification, the undoped CQWs covered with oleic acid ligands are dispersed in hexane. As shown in the left panel of **Figure 1**a, the quantum confinement in the vertical direction of undoped CQWs enables two sharp excitonic transitions, which correspond to the electron/light-hole (maxima at 480 nm) and electron/heavy-hole (maxima at 512 nm) absorption features (top panel of Figure 1b). Due to the ultrafast relaxation of light-holes to heavy-holes (<1 ps),[25,26] only greenish BE emission peaked at 514 nm associated with electron/heavy-hole exciton recombination can be observed in the emission spectrum (the top panel of Figure 1b). Imaging by transmission electron microscopy (TEM) shows that the undoped CQWs have a monodisperse size distribution and a flat square-like shape with an average size of 22 ± 5 nm (Figure S1a, Supporting Information), supporting the formation of long-range ordered superlattices.

Copper ions doped into CdSe CQWs can be realized by using both nucleation doping and partial cation exchange.[22,27–30] However, the nucleation doping method generally results in rectangular-shaped CQWs which are difficult for long-range stacking. For this work, we prefer doped and undoped CQWs with similar dimensions to construct the binary superlattice, therefore, we follow our earlier report on partial cation exchange recipes, where we add a controllable amount of copper acetate precursor into a solution of square-shaped undoped four ML core CQWs.[28] It is worth mentioning that under the studied doping range, copper dopants modify neither the geometry of the CQWs (Figure S1b, Supporting Information) nor the essential excitonic absorbance of the CQWs. One can see in the bottom panel of Figure 1b, both electron/heavy-hole and electron/light-hole transitions remain unchanged. Here, the role of copper dopants is to introduce emissive midgap states into the CQW host, as shown in the right panel of Figure 1a. After photoexcitation, the heavy-holes can be trapped

by the copper sites ($Cu^{1+} + h \rightarrow Cu^{2+}$, h denotes the heavy-hole), and then CE (a broad reddish emission band in the bottom panel of Figure 1b) is activated by the recombination between the captured holes in copper dopants and the electrons in the conduction band of the host CQWs: $Cu^{2+} + e \rightarrow Cu^{1+} + h\nu$ ($h\nu$ is the photon energy of CE and e denotes an electron).[23,31,32]

We mix the undoped and Cu-doped CQWs dispersed in hexane (the concentration of both is 10 mg mL^{-1}) into a total of ≈3 mL volume with an undoped-to-doped molar ratio of 10. Previously, various groups (e.g., Dubertret,[9,10] Demir,[17,20] and Abécassis[33]) have demonstrated that adding polar solvents such as ethanol into the CQW dispersions, which are dissolved in nonpolar solvents (such as hexane here), can lower the interaction potentials between the platelet planes of CQWs because the nonpolar capping ligands will force the CQWs to minimize the surface energy to draw away these added polar solvents.[13,20] Therefore, a relatively strong van der Waals attraction between the platelet planes induces the CQWs to stack on top of each other and results in a column-like superlattice.

Here, we adopt the same method to initiate the stacking. To control the degree of stacking, different amounts of ethanol are added to the same pristine mixture. We observe that when a larger amount of ethanol is added into the binary mixture, after stirring for a while, the solution becomes more turbid, suggesting the formation of macroscale particles.[9] More interestingly, by tuning the volume of added ethanol, the emission colors of the binary mixture can be modified. Specifically, under UV illumination as shown in Figure 1c, the pristine mixture is greenish since the majority of emitters are undoped CQWs; however, the color of the mixture changes from green to red with more ethanol added, indicating that CE is dominating the emission process. Note that all these four solutions look yellowish under room light. At this point, a legitimate question would be whether the added ethanol changes the intrinsic properties of CQWs. To rule out this possibility, we have investigated again the absorption and emission spectra of the mixtures after adding ethanol. The results in Figure S2 (Supporting Information) reveal that: two excitonic transition features are still located at 480 and 512 nm. Also, the peak position as well as the full-width at half-maximum (FWHM) of both BE and CE display negligible changes. The only changing factor is the intensity ratio between CE and BE. Thus, we can attribute the observed modification to the formation of superlattices.

To better understand the formation of CQW superlattices and characterize the degree of stacking, TEM images of the mixtures with different amounts of ethanol addition are exhibited in Figure 1d. For the pristine mixture (i.e., no ethanol added, see the left TEM panel), all CQWs are in the face-down configuration and no discernible stacking can be observed. When 100 µL of ethanol is added into the mixture (see the middle TEM panel), sparsely microwire-like superlattices, in which CQWs are edged-up in a highly aligned columnar order and the principal axis of the superlattice (i.e., the axis along the superlattice) is perpendicular to the platelet plane of CQWs, are detected. As the volume of ethanol increased to 400 µL (see the right TEM panel), we notice that almost all CQWs are assembled into the stacking manner to form the superlattices. Even in the direction parallel to the platelet plane of
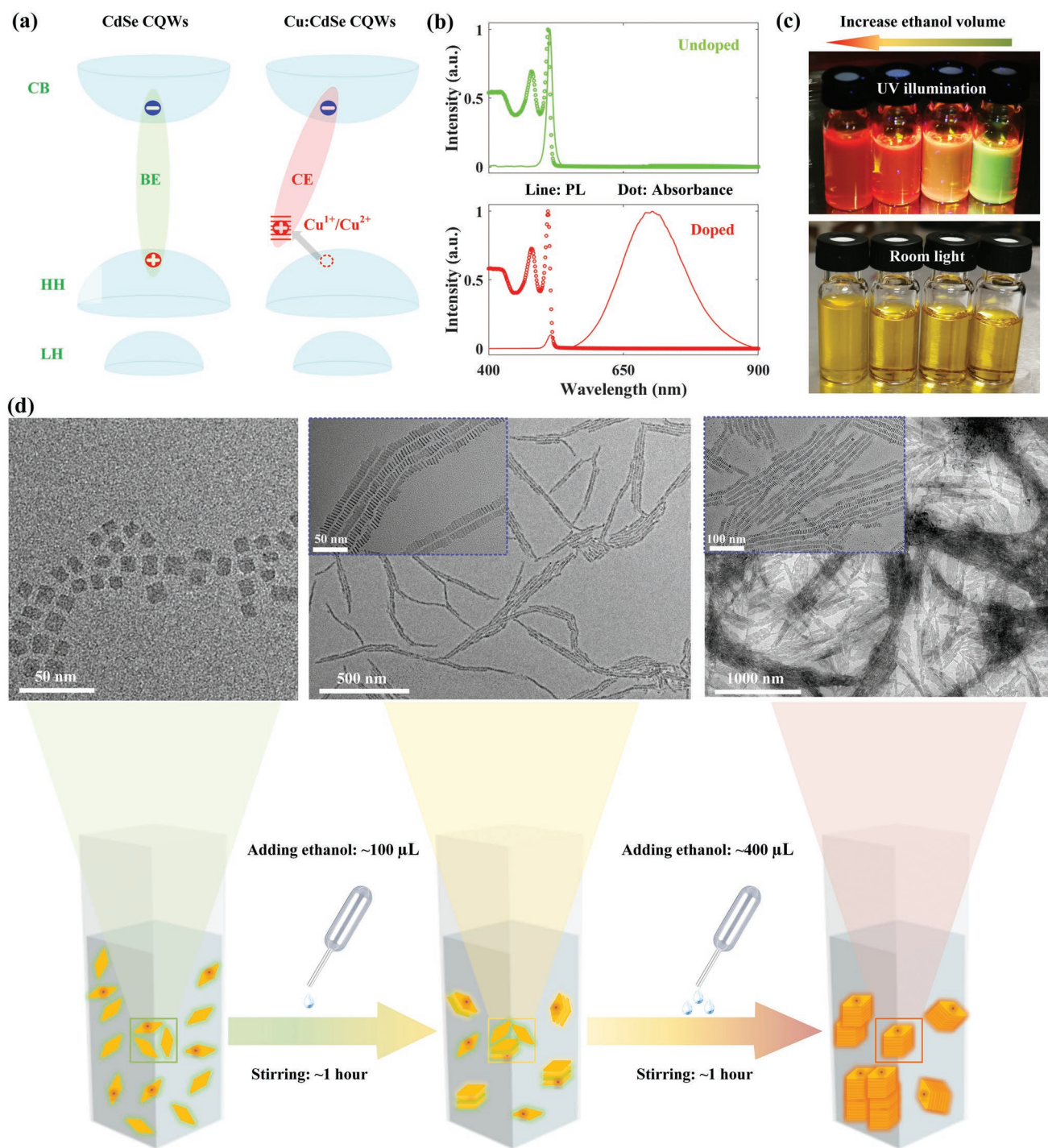
Figure 1. Formation of binary CQW superlattices. a) Schematic illustrations of the excitonic processes in undoped CQWs (left panel) and Cu-doped CQWs (right panel). CB: conduction band, HH: heavy-hole, LH: light-hole. b) Absorption and photoluminescence spectra of undoped CQWs (top panel) and Cu-doped CQWs (bottom panel). c) Color pictures of the binary CQW mixture dispersed in hexane with different amounts of added ethanol under 365 nm UV lamp (top panel) and under room light (bottom panel). From right to left: the volume of ethanol added into the binary mixture is 0, 100, 200, and 400 µL, respectively. d) Schematic of adding ethanol to obtain CQW superlattices with different stacking degrees and corresponding TEM images of the binary CQWs. As the volume of ethanol is increased gradually, longer and heavier stacking of CQWs into columnar superlattices is observed.

CQWs, more than ten columns of stacked CQWs with a width larger than 100 nm are standing side by side to form a giant superlattice. It is worth mentioning that small-angle X-ray scat-

tering (SAXS) measurements can further confirm the formation of the ordered superlattice and extract the average center-to-center distance between two adjacent CQWs.[9,33–35]
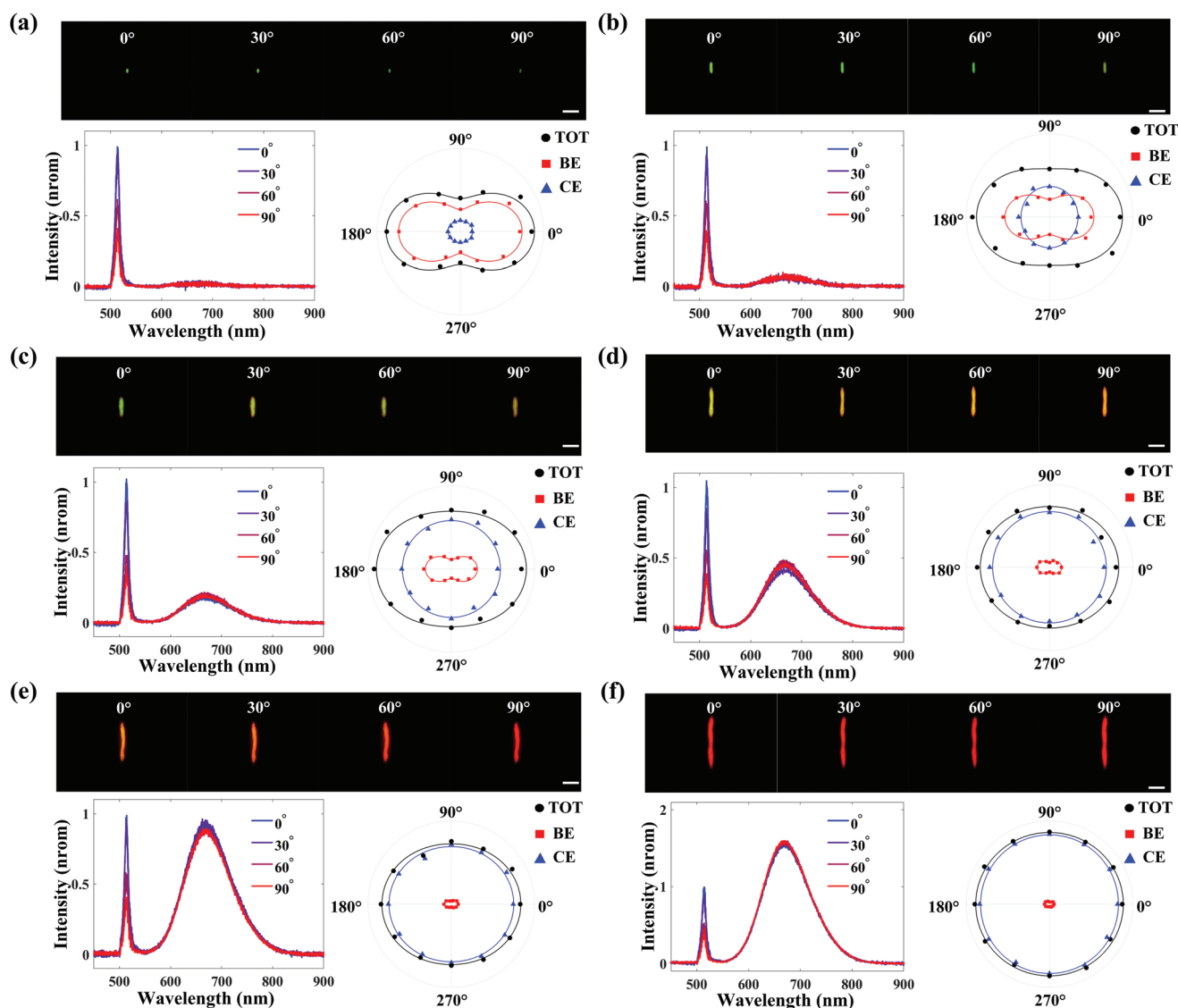
ADVANCED
SCIENCE NEWS
www.advancedsciencenews.com

ADVANCED
OPTICAL
MATERIALS
www.advopticalmat.de

Figure 2. Emission color and anisotropy in the binary CQW superlattices with different stacking lengths. Photoluminescence microscopy images (above), angle-dependent emission spectra (lower-left panel), and angular polarization profiles of emission (lower right panel) of the binary superlattice with a length of a–f) ≈1.4, ≈3.8, ≈6.7, ≈9.8, ≈13.4, and ≈17.2 µm, respectively. All are excited by a continuous-wave laser (405 nm) with a linear polarization perpendicular to the principal axis of superlattices. The angle between detection polarization and excitation polarization is indicated. In the emission images, the scale bar is 5 µm. The plotted data in angular profiles are fitted with a sinusoidal function. TOT: normalized integrated intensities of the full (total) emission spectra.

At the aim of providing convincing evidence that the controllability is resulting from the formation of superlattices, it is essential to extract the emission properties of a single superlattice from the ensemble photoluminescence (PL) profile of the dispersion which contains multiple superlattices with different stacking levels.[36] To ensure only an individual superlattice is characterized, after adding 200 µL ethanol, a diluted binary mixture dispersion is sparsely deposited onto a glass substrate via drop-casting. Then, each specific superlattice is excited by a linearly-polarized continuous-wave laser (405 nm) with polarization perpendicular to the principal axis of the superlattice, i.e., parallel to platelet planes. The emission is collected by an angle-resolved polarized µ-PL setup (see experimental details in the Experimental Section) to probe the color and anisotropy.[9,37,38]

Six superlattices with different stacking lengths have been characterized and the optical images recorded by a CMOS camera allow us to determine the length value. The results of superlattices with lengths of 1.4, 3.8, 6.7, 9.8, 13.4, and 17.2 µm are presented in **Figure 2**. The emission images and spectra of the single superlattice have exhibited consistency with our previous observation in superlattice dispersion (Figure 1c and Figure S2, Supporting Information): the stacking length can modify the intensity ratio between BE/CE and a longer superlattice will display the emission color closer to red. Great attention is paid to the angle-resolved polarized emission properties (see the angular polarization profiles in the lower right panel of Figure 2). For all these six superlattices with different stacking lengths, we find that there is a periodical oscillation of the BE
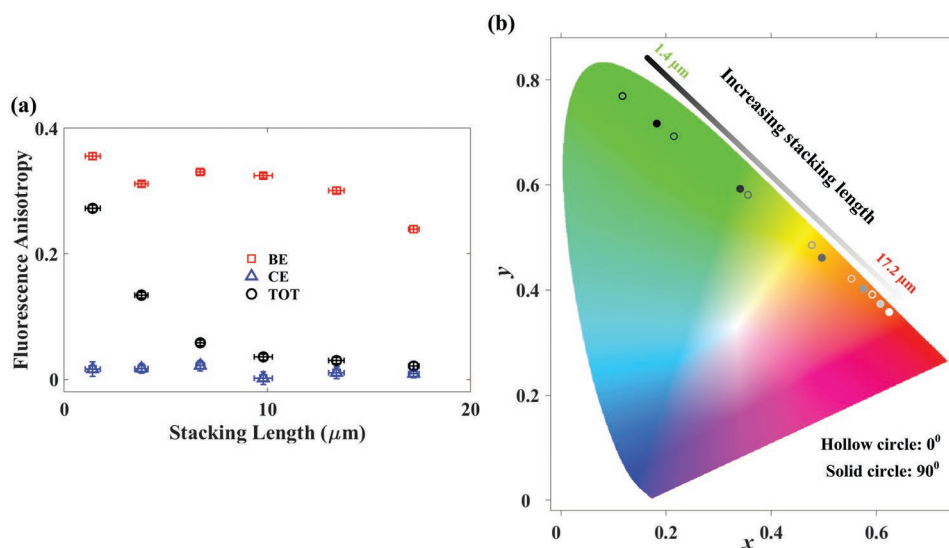
**ADVANCED
SCIENCE NEWS**

www.advancedsciencenews.com

**ADVANCED
OPTICAL
MATERIALS**

www.advopticalmat.de

Figure 3. A summary of the achieved controllability. a) Anisotropy as a function of stacking length for BE, CE, and full emission spectra. b) Corresponding color gamut of the emission colors from the superlattice with different stacking lengths when the polarizer is perpendicular to the principal axis of the superlattice (0°, the hollow circles) and the polarizer is parallel to the principal axis of the superlattice (90°, the solid circles).

intensity with respect to polarization angle; and in striking contrast, no periodical variation of CE intensity is observed.

This discrepancy stems from the different preferences of the transition dipole orientation in BE and CE. It has been widely reported that the electron/heavy-hole exciton transition dipoles in CdSe CQWs are near-perfectly oriented in the platelet plane.[12,13] This pure in-plane dipole orientation can be understood by using the band-edge periodic function ($|u\rangle$). With spin–orbit interaction (here we define the quantum confinement along Z-direction), conduction band electrons have s-like symmetry and $|u_e\rangle$ can be written as $|1/2, \pm1/2\rangle$, while heavy-holes hold p-like symmetry and $|u_{\text{heavy-hole}}\rangle$ takes $|3/2, \pm3/2\rangle$. We will find that the transition strength (the integral of $\langle u_e|\mu|u_{\text{heavy-hole}}\rangle$) can only be non-zero for dipoles oriented in the platelet plane (i.e., the X–Y plane).[12] Consequently, in the edge-up configuration (i.e., all platelet planes of CQWs are perpendicular to the substrate and the principal axis in the superlattice), BE (the radiative recombination of electron/heavy-hole exciton) will be the brightest when the principal axis of superlattices is perpendicular to the collection polarizer ($I_{0°}$, the collection polarization is parallel to the excitation polarization) and be the weakest when the principal axis of superlattices is parallel to the collection polarizer ($I_{90°}$, the collection polarization is perpendicular to the excitation polarization).

While for CE (the radiative recombination between the trapped holes and electrons in the host conduction band), transition dipoles do not have any preference and isotropic emission is expected since after the hole is trapped by the copper sites, the Z-projection of total angular momentum is not fixed at $\pm3/2$ anymore and the in-plane conservation has been broken. Similar interpretations can be found in the light-holes ($|u\rangle = |3/2, \pm1/2\rangle$) and spinoff-holes ($|u\rangle = |1/2, 1/2\rangle$), in which the dipole orientation is projected in all space directions.[12] We can also calculate the anisotropy value (R) of BE and CE using:[19,37–39] $(I_{0°} - I_{90°})/(I_{0°} + 2 \times_{90°})$ to quantize the contrast. As shown in **Figure 3**a, CE yielded an anisotropy value of nearly

zero, indicating no net anisotropy (i.e., isotropy). While for BE, with a short stacking length, the anisotropy value is above 0.3, which is comparable to the results in colloidal nanorods;[19,39] with longer stacking length, the anisotropy value decreases to ≈0.2 possibly because CQWs are harder to maintain pure edge-up configurations in such a long chain (over 15 μm). Benefitting from the huge anisotropy value contrast in BE/CE, modification of full-spectrum anisotropy will be concomitantly achieved when the intensity ratio between CE and BE is tuned by the stacking length. In Figure 3a, we can see that in the short-stacked superlattice, the full-spectrum is highly anisotropic since BE is dominating the emission spectra, and by the increase of stacking length, the total emission of the superlattice becomes almost isotropic. Moreover, colour coordinates of the two polarizations of emission spectra for six superlattice lengths are plotted in the CIE 1931 chromaticity diagram (Figure 3b), which shows impressive color controllability ranging from green to red. It is worth mentioning that if proper filters are adopted, such as polarization filters, one can further enhance the color purity by utilizing the contrast anisotropy values of BE and CE.

After demonstrating the capability of the stacking length to modify the collective emission color and anisotropy in superlattices, the remaining task is to clarify the underpinning physics that enable the controllability. Based on our knowledge of CdSe CQWs from previous works, the most reasonable hypothesis is that the exciton sinking in the Cu-doped CQWs (associated with CE) is boosted by efficient and long-range exciton transfer in superlattices. Let us start with the superlattice constructed by pure undoped CdSe CQWs. Due to the physically close dipole–dipole interaction (various groups have reported a spatial period of <5 nm in CdSe CQW stacking[11,17,20,22]), pure in-plane dipole orientation and a large self-overlap between the emission/absorption spectra, photoexcited band-edge excitons could transfer back and forth among the adjacent CQWs via Förster resonance energy transfer (FRET), which is a nonradiative
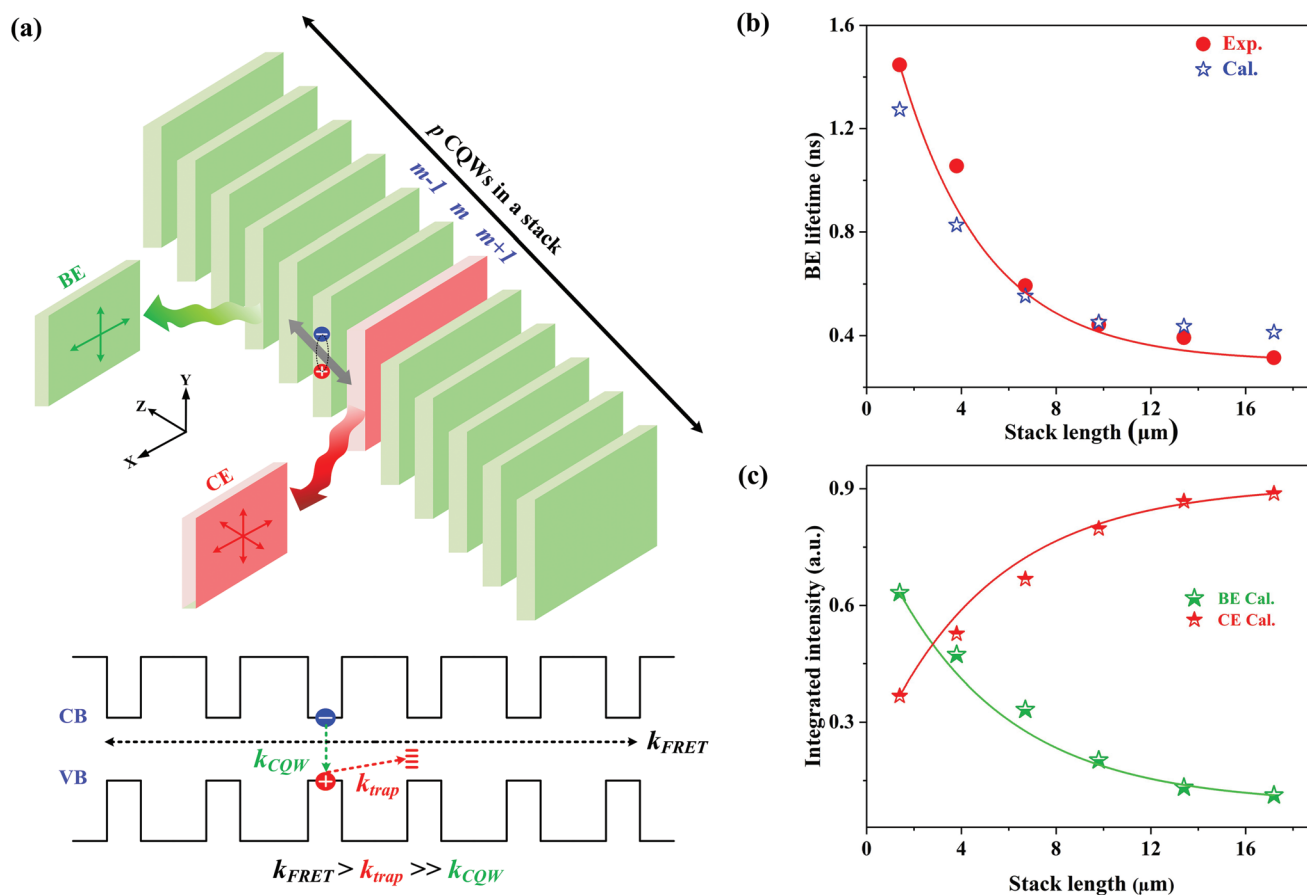
**ADVANCED
SCIENCE NEWS**

www.advancedsciencenews.com

**ADVANCED
OPTICAL
MATERIALS**

www.advopticalmat.de

Figure 4. Controlling mechanism in the binary CQW superlattice. a) Schematic illustration of FRET assisted exciton trapping process in the binary superlattice. Green shaded plates denote undoped CQWs in which BE is greenish and anisotropic due to the in-plane dipole orientation. While red shaded plates represent Cu-doped CQWs in which CE is reddish and isotropic due to the lack of dipole orientation preference. Among all these exciton dynamics, exciton transfer via FRET is the fastest: k_{FRET} is ($\approx$3 ps)$^{-1}$ and exciton trapping by copper sites has the lifetime of several tens of picosecond (k_{trap}), the slowest process is band-edge exciton recombination (k_{CQW}), which is in the nanosecond range. b) Correlating the simulated BE lifetime (the hollow stars) with the experimental value (the solid circles) to determine the fraction of the Cu-doped CQW population in the superlattice. The red line is a guide to the eye. c) The calculated BE/CE intensity with various stacking lengths. The agreeable trend exhibits very good support for our mechanism interpretation. The two solid lines are the guides to the eye.

exciton transfer process via near-field dipolar coupling. Rowland et al. in 2015[15] and Guzelturk et al. in 2014[20] reported that the exciton transfer in CdSe CQW stacking can be as fast as $\approx$3 ps with a near-unit efficiency and outpace the Auger recombination. Considering the lifetime of band-edge recombination is around 3 ns, excitons can hop about a thousand times in the column-like assembly before annihilation.

Now we insert the Cu-doped CQWs which behave as the exciton trappers into the stacks, as shown in the schematic illustration in **Figure 4**a, taking advantage of the multiple transfer loops of band-edge excitons, the copper sites with a hole trapping lifetime of several tens picosecond[23,31] could capture tremendous photo-excited excitons generated in both doped and undoped CQWs. The scenario in our study is an emissive analogue to previous observations that demonstrated emission of chromophores or nanocrystals is quenched in the assembly due to non-emissive trapping assisted by homo-FRET.[17,20,40] As the stacking length is getting longer (i.e., the number of Cu-doped CQWs in the stacking is larger), more of the band-edge excitons will be affected by the exciton trapping

process boosted by exciton transfer. As a result, the excitation energy is more likely to be released through the CE channel. We have checked the BE dynamics (probed at 514 nm) of non-stacking CQWs and stacking CQWs with different lengths to support our argument (Figure S3, Supporting Information). The CQWs have an $\approx$2.42-ns average emission lifetime before stacking is induced, which is in accordance with other four ML CdSe CQWs reports.[13,17,25] As the superlattice is formed, the average BE lifetime can decrease by an order of magnitude to $\approx$320 ps for the longest stacking. This indicates that the new band-edge exciton consuming channel (i.e., exciton trapping) becomes much stronger with the increase of stacking length.

To further confirm our inference and develop a deeper understanding, we perform a kinetic simulation based on a set of rate equations[17,20,41,42] to reproduce the observed controllability (see the simulation details in Note S1, Supporting Information). For simplicity, we assume the fraction (f) of the Cu-doped CQW population within the whole CQW population in all superlattices is fixed (because the superlattice constructed from the uniformly mixed dispersion, the stacking with a con-

siderable amount of CQWs should contain a similar population percentage of doped ingredient) and there is no nonradiative loss in the superlattice. To extract the f value in our experiments, we have swept this parameter from 0.01 to 0.20 to correlate the simulated BE dynamics with the measured BE decays in Figure S3 (Supporting Information) and found acceptable accordance when $f = 0.13$ (as shown in Figure 4b). Then we can determine the photoexcited energy-releasing via BE and CE channels: the BE energy is calculated by integrating the simulated BE dynamics in a relatively long-time window while the CE energy is obtained by subtracting BE photons from the photoexcited photons. The stacking-length-dependent BE/CE intensity from the kinetic model is shown in Figure 4c. Note that we do not expect to achieve good quantitative matching between experiment and simulation results due to the simplification of the model and the random nature of the stacking process. Nevertheless, our simulation results exhibit a good trend in agreement with experimental results: a longer stacking length results in more photoexcited energy released via the CE channel and the collective emission of the superlattice becomes more reddish and isotropic. This again supports our hypothesis that FRET assisted exciton trapping is the dominating mechanism for the collective emission property control.

3. Summary

In summary, we have proposed and demonstrated that the emission properties in a host–guest superlattice consisting of undoped and Cu-doped CQWs are highly controllable through a solvent engineer approach. The physical origin of the controllability lies in the exciton hopping boosted exciton trapping process. As the vertical dimension increases, the ultra-efficient homo-FRET leads to more excitons sinking into the Cu-doped CQWs. Therefore, the copper emission, which is reddish and isotropic, gradually overwhelms the band-edge emission, which is greenish and anisotropic. Moreover, a kinetic model has been developed, which strongly agrees with the observed modulation in our experiments. Given the simplicity and flexibility in tuning collective properties of the superlattice, we anticipate that our work could be, in the future, exploited for practical photonic applications.

4. Experimental Section

Steady-State Optical Properties of Cu-Doped and Undoped Dispersion: Absorption spectra of CQWs in hexane were measured by a UV–vis spectrophotometer (Shimadzu, UV-1800). PL spectra of CQWs in hexane were recorded using a spectrofluorophotometer (Shimadzu, RF-5301PC, excitation wavelength: 355 nm).

Characterization of Emission Color and Anisotropy in Binary CQW Superlattice: The excitation source is a 405-nm continuous-wave laser (Cobolt 06-MLD), and the laser spot was focused into the superlattice by a microscope objective (ZEISS, NA = 0.65). The linear excitation polarization was achieved by using the combination of a linear polarizer and a $\lambda/2$ wave-plate. The glass substrate hosting superlattices was mounted in a motion stage, which can move along X- and Y-direction to bring different superlattices with various stacking lengths into the field of view, and also can rotate to make sure the principal axis of the superlattice is perpendicular to the excitation polarization. The emission was collected by the same objective in the reflection geometry and the excitation laser was filtered out by a long-pass (LP) filter. Then the emission was passed through the collection polarizer and a 50/50 beam splitter, one path was recorded by a colorful CMOS camera and another path was into the fiber-coupled ANDOR spectrometer (monochromator: ANDOR Shamrock 303i, CCD: ANDOR iDus 401). By rotating the collection polarizer in front of the beam splitter, the angle-dependent emission color and anisotropy can be probed.

Time-Resolved Photoluminescence in Binary CQW Superlattice: The time-resolved PL spectroscopy was performed with a Becker & Hickl DCS 120 confocal scanning FLIM system with the laser pulse at 375 nm with the repetition rate of 20 MHz. For all the time-resolved PL measurements, the collection time is 180 s. Third-order exponential decay models were used to fit the emission dynamics in Figure S6 (Supporting Information) and the instrument response function (IRF) was deconvoluted during the fitting.

Supporting Information

Supporting Information is available from the Wiley Online Library or from the author.

Conflict of Interest

The authors declare no conflict of interest.

Author Contributions

J.Y. and M.S. contributed equally to this work. C.D. and H.V.D. supervised and contributed to all aspects of the research. J.Y. initiated the idea and discussed experiments with M.S. and C.D. in detail. J.Y. wrote the manuscript with the inputs from all authors. With inputs from H.V.D., M.S. designed the doped CQWs and A.S. performed the material synthesis. J.Y. and M.S. performed the experiments to control the degree of stacking. S.D. and H.D.B. conducted the TEM measurement to characterize the stacking. J.Y. and Y.W. conducted the steady-state and dynamic spectroscopy measurements. J.Y. and C.D. performed the kinetic model simulation. All authors analyzed the data, discussed the results, and commented on the manuscript.

Data Availability Statement

The data that support the findings of this study are available from the corresponding author upon reasonable request.

[1] Z. Nie, A. Petukhova, E. Kumacheva, *Nat. Nanotechnol.* **2010**, *5*, 15.

[2] E. V. Shevchenko, D. V. Talapin, N. A. Kotov, S. O'Brien, C. B. Murray, *Nature* **2016**, *439*, 55.

[3] D. V. Talapin, E. V. Shevchenko, M. I. Bodnarchuk, X. Ye, J. hen, C. B. Murray, *Nature* **2009**, *461*, 964.

[4] T. Wang, J. Zhuang, J. Lynch, O. Chen, Z. Wang, X. Wang, D. LaMontagne, H. Wu, Z. Wang, Y. C. Cao, *Science* **2012**, *338*, 358.

[5] Y. Nagaoka, H. Zhu, D. Eggert, O. Chen, *Science* **2018**, *362*, 1396.

[6] Y. Nagaoka, R. Tan, R. Li, H. Zhu, D. Eggert, Y. A. Wu, Y. Liu, Z. Wang, O. Chen, *Nature* **2018**, *561*, 378.

[7] S. Ithurria, M. D. Tessier, B. Mahler, R. P. S. M. Lobo, B. Dubertret, A. L. Efros, *Nat. Mater.* **2011**, *10*, 936.

[8] J. Yu, C. Dang, *Cell Rep. Phys. Sci.* **2021**, *2*, 100308.

[9] B. Abécassis, M. D. Tessier, P. Davidson, B. Dubertret, *Nano Lett.* **2014**, *14*, 710.

[10] M. D. Tessier, L. Biadala, C. Bouet, S. Ithurria, B. Abécassis, B. Dubertret, *ACS Nano* **2013**, *7*, 3332.

[11] C. E. Rowland, I. Fedin, H. Zhang, S. K. Gray, A. Govorov, D. V. Talapin, R. D. Schaller, *Nat. Mater.* **2015**, *14*, 484.

[12] R. Scott, J. Heckmann, A. V. Prudnikau, A. Antanovich, A. Mikhailov, N. Owschimikow, M. Artemyev, J. I. Climente, U. Woggon, N. B. Grosse, A. W. Achtstein, *Nat. Nanotechnol.* **2017**, *12*, 1155.

[13] Y. Gao, M. C. Weidman, W. A. Tisdale, *Nano Lett.* **2017**, *17*, 3837.

[14] J. Yu, S. Hou, M. Sharma, Y. M. Tobing, Z. Song, S. Delikanli, C. Hettiarachchi, D. Zhang, W. Fan, M. D. Birowosuto, H. Wang, H. V. Demir, C. Dang, *Matter* **2020**, *2*, 1550.

[15] T. Paik, D.-K. Ko, T. R. Gordon, V. Doan-Nguyen, C. B. Murray, *ACS Nano* **2011**, *5*, 8322.

[16] X. Ye, J. Chen, M. Engel, J. A. Millan, W. Li, L. Qi, G. Xing, J. E. Collins, C. R. Kagan, J. Li, S. C. Glotzer, C. B. Murray, *Nat. Chem.* **2013**, *5*, 466.

[17] O. Erdem, M. Olutas, B. Guzelturk, Y. Kelestemur, H. V. Demir, *J. Phys. Chem. Lett.* **2016**, *7*, 548.

[18] R. Momper, H. Zhang, S. Chen, H. Halim, E. Johannes, S. Yordanov, D. Braga, B. Blülle, D. Doblas, T. Kraus, M. Bonn, H. I. Wang, A. Riedinger, *Nano Lett.* **2020**, *20*, 4102.

[19] P. D. Cunningham, J. B. Souza, I. Fedin, C. X. She, B. Lee, D. V. Talapin, *ACS Nano* **2016**, *10*, 5769.

[20] B. Guzelturk, O. Erdem, M. Olutas, Y. Kelestemur, H. V. Demir, *ACS Nano* **2014**, *8*, 12524.

[21] M. A. Boles, M. Engel, D. V. Talapin, *Chem. Rev.* **2016**, *116*, 11220.

[22] J. Yu, M. Sharma, S. Delikanli, M. D. Birowosuto, H. V. Demir, C. Dang, *J. Phys. Chem. Lett.* **2019**, *10*, 5193.

[23] H. D. Nelson, X. Li, D. R. Gamelin, *J. Phys. Chem. C* **2016**, *120*, 5714.

[24] S. Ithurria, B. Dubertret, *J. Am. Chem. Soc.* **2008**, *130*, 16504.

[25] M. Pelton, S. Ithurria, R. D. Schaller, D. S. Dolzhnikov, D. V. Talapin, *Nano Lett.* **2012**, *12*, 6158.

[26] L. Biadala, F. Liu, M. D. Tessier, D. R. Yakovlev, B. Dubertret, M. Bayer, *Nano Lett.* **2014**, *14*, 1134.

[27] M. Sharma, K. Gungor, A. Yeltik, M. Olutas, B. Guzelturk, Y. Kelestemur, T. Erdem, S. Delikanli, J. R. McBride, H. V. Demir, *Adv. Mater.* **2017**, *29*, 1700821.

[28] M. Sharma, M. Olutas, A. Yeltik, Y. Kelestemur, A. Sharma, S. Delikanli, B. Guzelturk, K. Gungor, J. R. McBride, H. V. Demir, *Chem. Mater.* **2018**, *30*, 3265.

[29] J. Yu, M. Sharma, M. Li, S. Delikanli, A. Sharma, M. Taimoor, Y. Altintas, J. R. McBride, T. Kusserow, T. C. Sum, H. V. Demir, C. Dang, *Laser Photonics Rev.* **2021**, *15*, 2100034.

[30] J. Yu, M. Sharma, M. Li, P. L. Hernandez-Martinez, S. Delikanli, A. Sharma, Y. Altintas, T. C. Sum, H. V. Demir, C. Dang Sustained biexciton emission in colloidal quantum wells assisted by dopant-host interaction. arXiv 2019, 1905.11571.

[31] K. E. Hughes, K. H. Hartstein, D. R. Gamelin, *ACS Nano* **2018**, *12*, 718.

[32] V. Pinchetti, Q. Di, M. Lorenzon, A. Camellini, M. Fasoli, M. Zavelani-Rossi, F. Meinardi, J. Zhang, S. A. Crooker, S. Brovelli, *Nat. Nanotechnol.* **2018**, *13*, 1145.

[33] S. Jana, M. de Frutos, P. Davidson, B. Abécassis, *Sci. Adv.* **2017**, *3*, e1701483.

[34] S. Jana, P. Davidson, B. Abecassis, *Angew. Chem.* **2016**, *128*, 9517.

[35] S. Jana, T. N. T. Phan, C. Bouet, M. D. Tessier, P. Davidson, B. Dubertret, B. Abecassis, *Langmuir* **2015**, *31*, 10532.

[36] J. Cui, A. P. Beyler, I. Coropceanu, L. Cleary, T. R. Avila, Y. Chen, J. M. Cordero, S. L. Heathcote, D. K. Harris, O. Chen, J. Cao, M. G. Bawendi, *Nano Lett.* **2016**, *16*, 289.

[37] E. Cassette, B. Mahler, J.-M. Guigner, G. Patriarche, B. Dubertret, T. Pons, *ACS Nano* **2012**, *6*, 6741.

[38] M.-J. Sun, Y. Liu, Z. Wei, Y. S. Zhao, Y.-W. Zhong, J. Yao, *J. Am. Chem. Soc.* **2019**, *141*, 6157.

[39] Y. Li, H. Huang, Y. Xiong, A. F. Richter, S. V. Kershaw, J. Feldmann, A. L. Rogach, *ACS Nano* **2019**, *13*, 8237.

[40] B. Guzelturk, M. Olutas, S. Delikanli, Y. Kelestemur, O. Erden, H. V. Demir, *Nanoscale* **2015**, *7*, 2545.

[41] J. Yu, M. Sharma, A. Sharma, S. Delikanli, H. V. Demir, C. Dang, *Light: Sci. Appl.* **2020**, *9*, 27.

[42] J. Yu, S. Shendre, W.-K. Koh, B. Liu, M. Li, S. Hou, C. Hettiarachchi, S. Delikanli, P. Hernandez-Martínez, M. D. Birowosuto, H. Wang, T. Sum, H. V. Demir, C. Dang, *Sci. Adv.* **2019**, *5*, eaav3140.